MATERIALS
CHEMISTRY
FRONTIERS

RESEARCH ARTICLE

Steering the luminescence of donor–acceptor materials by regioisomerism of triazole linkers

Laura Holzhauer, [ID] [a] Carolina Francener, [ID] [b] David Elsing, [ID] [c] Andrew Danos, [ID] [bd] Olaf Fuhr, [ID] [ce] Nicole Jung, [ID] [aef] Wolfgang Wenzel, [ID] [c] Andrew P. Monkman, [ID] [b] Stefan Bräse, [ID] [af] Mariana Kozlowska [ID] *[c] and Emma V. Puttock [ID] *[af]

We examine the impact of triazole connectivity on the photophysical properties of donor–acceptor emitters. In these systems, the electron donor is connected either to the triazole's nitrogen atom (N1, "N-connected") or carbon atom (C4, "C-connected"), giving rise to regioisomeric pairs with distinct excited-state behaviours. Donor strength and triazole orientation together govern energy levels, charge-transfer character, and delayed emission pathways. N-connected derivatives exhibit higher singlet energies and lower triplet energies compared to their C-connected counterparts, resulting in consistently larger ΔE_{ST} values. These trends are attributed to disrupted donor–acceptor conjugation through the nitrogen linkage, thereby rendering the acceptor less electron-deficient in the N-connected series. Most compounds favour room-temperature phosphorescence (RTP) due to large singlet–triplet energy gaps ($\Delta E_{ST} > 0.4$ eV), while phenoxazine C-connected (PXZ-C) uniquely exhibits thermally activated delayed fluorescence (TADF), attributed to its small ΔE_{ST} of 0.1 eV. Computational studies support these experimental trends, showing that the lowest triplet state is predominantly localised on the quinoxaline acceptor. These findings highlight the critical role of regioisomeric control in tuning excited-state dynamics in TADF materials.

Introduction

Organic emitters that can manage triplet excitons are the current focus of many areas of optoelectronics research, with advanced applications across OLEDs,[1] lasing,[2] sensing,[3] and more. Because of the low dielectric constant of organic materials,[4–6] managing the energies of 'tightly bound' singlet and triplet excitons is crucial to allow them to interconvert and support desired material functionality, *i.e.* triplet harvesting. The specific energies of singlet and triplet excitons emerge as consequences of the electronic structure of the molecules of interest, which empowers molecular design as the primary factor advancing progress in the properties and applications

of these materials. For materials featuring charge transfer (CT) states, the energies of the excited states are particularly sensitive to the choices of donor or acceptor fragment[7] or their specific bonding pattern,[8,9] and many examples now exist wherein the type of delayed emission and its particular properties can be explained in terms of these structural factors.[8–17]

Quinoxalines are widely recognised as effective acceptor units in the design of efficient thermally activated delayed fluorescence (TADF) organic emitters.[18–26] Organic light-emitting diodes (OLEDs) incorporating quinoxaline-based materials exhibit impressive external quantum efficiencies (EQE) of 39.1% for green OLEDs,[24] up to 30.3% for deep-red OLEDs,[21] and 16.7% for solution-processed red OLEDs.[18] These results highlight the potential of quinoxaline-based donor–acceptor systems as a promising direction for efficient TADF emitters.

Separately, triazoles are most commonly synthesised *via* copper-catalyzed azide–alkyne cycloadditions (CuAAC) and have been widely utilised as 'click chemistry' linkers for conjugated fluorophores.[27–30] When combined with heterocyclic structures, two common regioisomers can be distinguished based on how the triazole connects to the donor and acceptor units (see Fig. 1). Specifically, the N1 atom of the triazole moiety can link to the electron donor (referred to here as the 'N-connected' isomer), or the C4 atom can link to the electron

[a] *Institute of Biological and Chemical Systems – Functional Molecular Systems, Karlsruhe Institute of Technology, Kaiserstraße 12, 76131 Karlsruhe, Germany. E-mail: emma.puttock@kit.edu*
[b] *Department of Physics, Durham University, DH1 3LE Durham, UK*
[c] *Institute of Nanotechnology, Karlsruhe Institute of Technology, Kaiserstraße 12, 76131 Karlsruhe, Germany. E-mail: mariana.kozlowska@kit.edu*
[d] *School of Physical and Chemical Sciences, Queen Mary University of London, Mile End Road, London E1 4NS, UK*
[e] *Karlsruhe Nano Micro Facility, Karlsruhe Institute of Technology, Kaiserstraße 12, 76131 Karlsruhe, Germany*
[f] *Institute of Organic Chemistry, Karlsruhe Institute of Technology, Kaiserstraße 12, 76131 Karlsruhe, Germany*
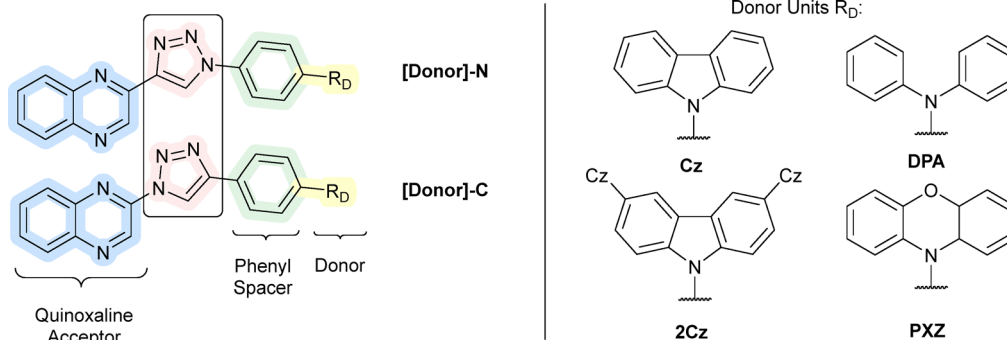
Fig. 1 Molecular design of quinoxaline-based donor–acceptor compounds connected through a triazole linker in orientation N-connected or C-connected.

donor ('C-connected' isomer). The orientation of the triazole substituent significantly affects intramolecular charge transfer, resulting in distinct photophysical properties for each regioisomer; for example, N-connected (regular) derivatives show red-shifted absorption and triazole-acceptor LUMO localisation compared to the more delocalised C-connected (inverted) series.[28] Studies on a series of porphyrin-fullerene and TPA-NDI dyes have shown that that C-connected triazole systems can facilitate enhanced donor–acceptor communication *via* delocalisation of the triazole nitrogen lone pair into the π-system.[31] In contrast, N-connected analogues lack this delocalisation pathway, limiting conjugation. The consequences of this in the context of CT materials featuring delayed emission involving triplet states has not been investigated.

To investigate the effects of triazole regioisomerism, we examined how the connection orientation and the donor unit type impact the luminescent properties of eight donor–acceptor systems using time-resolved emission spectroscopy. Quantum mechanical calculations of the ground and excited states yielded further insight into the charge transfer states, as well as the differences in low temperature and room temperature triplet emission. Ultimately we find that the regioisomerism of the triazole linker impacts both the singlet and triplet excited states, leading to a range of room-temperature phosphorescence (RTP) and TADF emission for compounds with different donor groups and connectivities.

Results and discussion

Synthesis and physical characterisation

To investigate how the triazole linker influences the photophysical properties of the molecule, we designed donor–acceptor systems incorporating an electron-deficient quinoxaline acceptor, an electron-rich donor unit, a phenyl spacer, and a triazole linker in two orientations: N-connected and C-connected (Fig. 1). The donor units, carbazole (**Cz**), 9,3′:6′,9″-tercarbazole (**2Cz**), diphenylamine (**DPA**), and phenoxazine (**PXZ**) were chosen to represent a range of compounds with varying donor strengths. The resulting compounds are denoted as **[Donor]-N** or **[Donor]-C**, corresponding to N-connected or C-connected
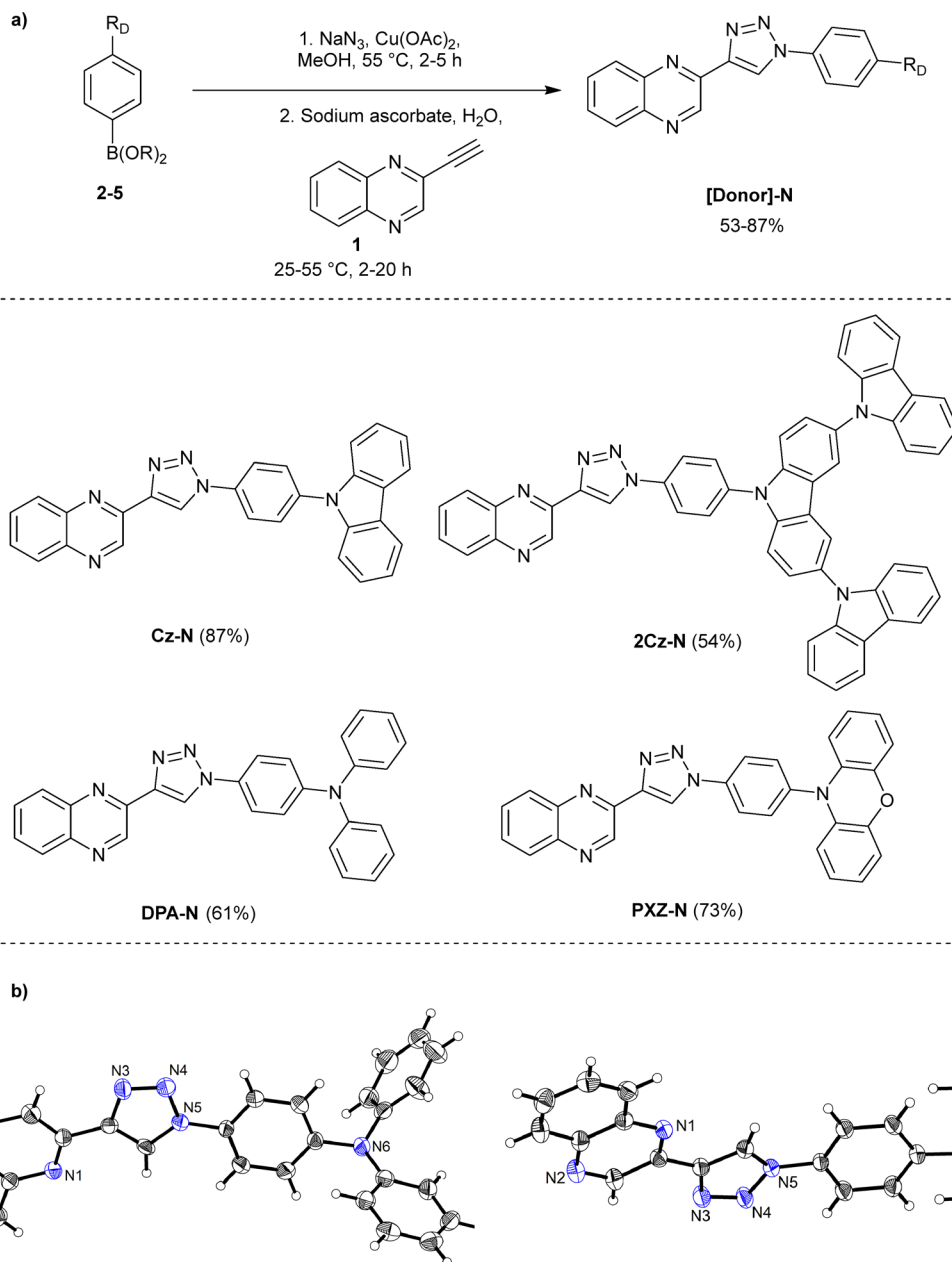
triazole linkers, respectively. For instance, **Cz-N** and **Cz-C** refer to carbazole donors with N- or C-connection, respectively.

To access N-connected derivatives, we employed a CuAAC reaction to couple 2-alkynylquinoxaline with donor moieties *via* a triazole linker (Scheme 1a). The precursor 2-alkynylquinoxaline (**1**) was synthesised through condensation, bromination, and Sonogashira cross-coupling, followed by alkyne deprotection (see SI, Scheme S1). Donor units functionalised with halogenated phenyl spacers (**2–5**) were prepared according to published procedures (Schemes S2–S4, SI). Using a one-pot CuAAC reaction, the target compounds, **[Donor]-N**, were obtained in yields of 53–87% and fully characterised, with molecular structures of **DPA-N** and **PXZ-N** confirmed *via* single-crystal XRD (Scheme 1b).

For C-connected derivatives, we employed two complementary synthetic strategies (Scheme 2a). Method A was used to synthesise **Cz-C**, **DPA-C** and **PXZ-C** by reacting alkyne-functionalised spacer-donor constructs (**7–9**) with tetrazolo-[1,5-*a*]quinoxaline (**6**) in a CuAAC reaction, yielding products in 54–70%. The preparation of the alkyne-functionalised spacer-donor constructs is detailed in the SI (Scheme S5). For the final compound, **2Cz-C**, Method B was applied (Scheme 2a; see also Scheme S6 in the SI). In this method, tetrazolo[1,5-*a*]-quinoxaline (**6**) was first reacted with a halogen-functionalised spacer-donor construct (**10**) *via* CuAAC to produce the intermediate **11**. Subsequently, intermediate **11** underwent a Hart-wig–Buchwald cross-coupling to attach the unmodified donor, yielding **2Cz-C** in a final yield of 44%. Both strategies enable access to donor-substituted triazolylquinoxalines, with method A preferred for higher yields and method B facilitating the use of complex donors.

The thermal stability of the N-connected and C-connected derivatives was assessed using thermogravimetric analysis (TGA), with **PXZ-N** and **PXZ-C** selected as representatives for comparison. A significant difference in the decomposition temperature (T_D) (weight loss of 5%) of compounds **PXZ-N** and **PXZ-C** was observed, with **PXZ-N** exhibiting a higher T_D compared to **PXZ-C**. The C-connected regioisomer displayed an initial decomposition stage, with weight decreasing from 98% to 92%, likely due to the loss of N_2, a feature absent in the N-connected regioisomer. Additionally, **PXZ-C** underwent faster decomposition overall, suggesting that the N-connected series

a)

Scheme 1 (a) Synthesis of N-connected derivatives. For the synthesis of derivative **2Cz-N**, an additional solvent mixture of DMF, EtOAc and toluene was added to fully dissolve the starting material. (b) ORTEP diagram of the molecular structure of **DPA-N** and **PXZ-N** with the thermal ellipsoids shown at 50% probability.

posesses greater thermal stability. Detailed TGA data, including decomposition temperatures and weight loss profiles, are provided in the SI (Fig. S1).
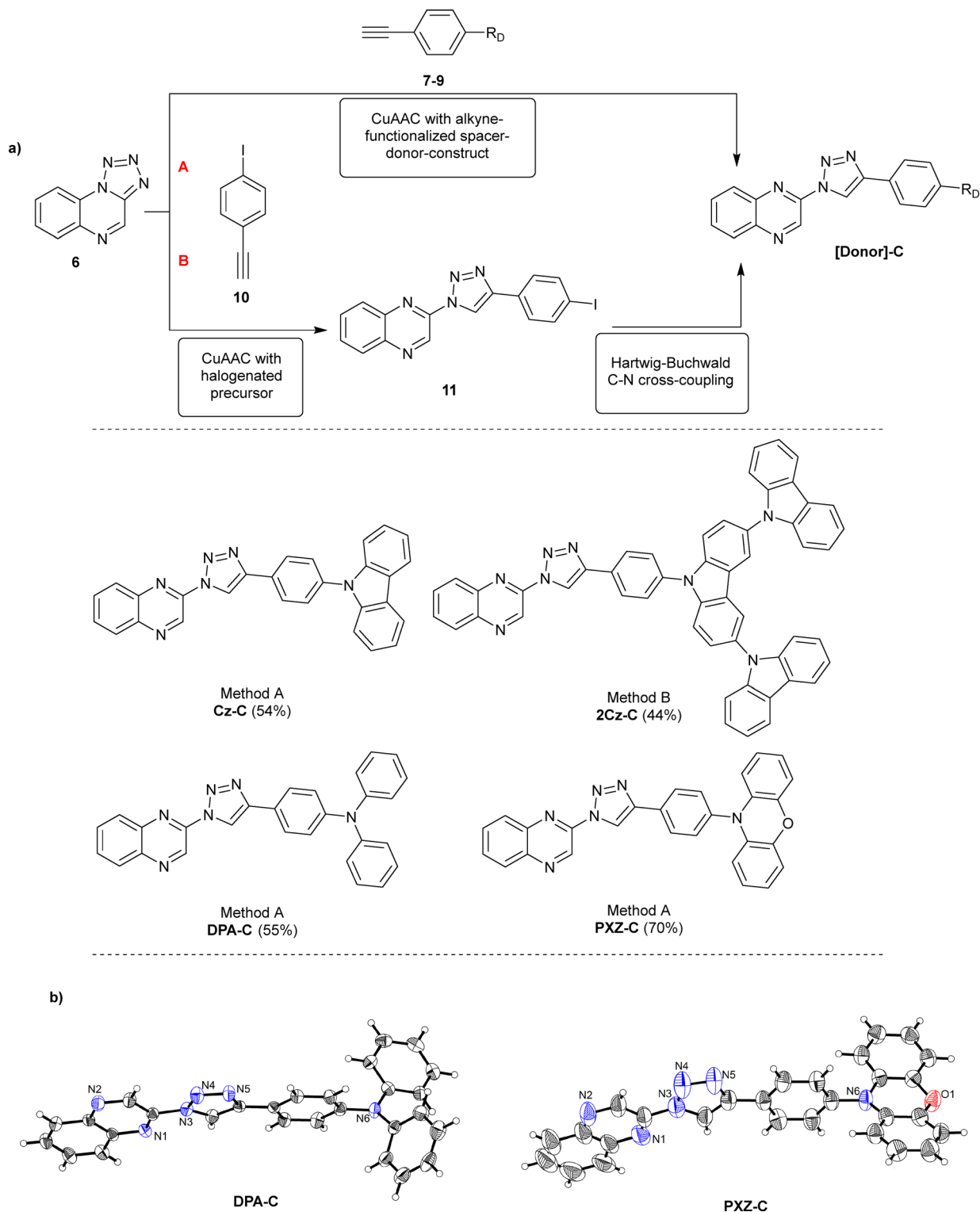
Electronic properties

The electrochemical properties of the emitter compounds were characterised *via* cyclic voltammetry (CV) in DCM (1 mM solutions) with Bu_4NPF_6 as the electrolyte salt. The HOMO and LUMO levels were approximated from the oxidation and reduction potentials, employing eqn (1):[32]

$$E_{\text{HOMO/LUMO}} = -(E_{\text{ox/red}} + 4.8) \text{ eV} \quad (1)$$

Both the HOMO and LUMO energies reflect the influence of donor strength and triazole connectivity. As expected, the oxidation potential, and therefore the HOMO level, is primarily determined by the donor. For instance, carbazole-substituted compounds showed deeper HOMO levels around −5.7 eV, while phenoxazine-substituted compounds displayed shallower HOMO levels around −5.1 eV. In contrast, the LUMO energy was more strongly affected by the nature of the triazole linkage. N-connected derivatives exhibited relatively consistent LUMO levels (−2.74 to −2.79 eV), regardless of the donor unit. In comparison, C-connected analogues showed more variation (−2.86 to −2.99 eV), with

Scheme 2 (a) Synthetic strategies **A** and **B** to assemble C-connected compounds. (b) ORTEP diagram of the molecular structure of **DPA-C** and **PXZ-C** with the thermal ellipsoids shown at 50% probability.

the LUMO energy depending more noticeably on the donor. This indicates that C-connection enhances donor–acceptor electronic communication, allowing the nature of the donor to play a greater role in LUMO stabilisation. The consistently lower LUMO levels in the C-connected series reflect this stronger interaction and are in agreement with computational results (see Table S2, SI). This differential tuning of HOMO and LUMO levels leads to a consistent narrowing of the HOMO–LUMO gap

Table 1 Summary of oxidation and reduction energies obtained *via* cyclic voltammetry and estimated HOMO/LUMO levels and HOMO−LUMO gaps

Compound	E_{ox} [V]	E_{red} [V]	HOMO [eV]	LUMO [eV]	Gap [eV]
Cz-N	0.97[a]	−2.01	−5.77	−2.79	2.98
Cz-C	0.93[a]	−1.89	−5.73	−2.91	2.82
DPA-N	0.63	−2.06	−5.43	−2.74	2.69
DPA-C	0.52	−1.94	−5.32	−2.86	2.46
PXZ-N	0.36	−2.03	−5.16	−2.77	2.39
PXZ-C	0.29	−1.91	−5.09	−2.99	2.10

[a] Calculated from irreversible oxidation feature.

in C-connected compounds relative to their N-connected analogues, as summarised in Table 1. Full CV traces are provided in the SI (Fig. S1). Compounds **2Cz-N** and **2Cz-C** were omitted from this analysis, as the large donor system produced multiple overlapping oxidation waves and almost no reproducible reduction, preventing accurate determination of HOMO and LUMO levels.

Photophysical properties

The UV-visible absorption spectra of aerated toluene solutions (10 μM) were investigated and are shown in Fig. S2, SI. In most cases, the absorption maxima wavelengths for the N-connected and C-connected derivatives with the same donor were nearly identical, with global maxima located around 290 and 340 nm. Generally, the N-connected regioisomers exhibited stronger absorption intensities compared to their C-connected counterparts. Additionally, peak positions were consistent within each connection type. However, an exception was observed for the DPA-substituted derivatives, where the lower-energy absorption maximum was significantly red-shifted to 386 nm for **DPA-C**, compared to 362 nm for **DPA-N**. To rationalise these differences, time-dependent density functional theory (TDDFT) calculations were performed. Using the optimized structures obtained with CAM-B3LYP/def2-TZVP,[33,34] we examined the nature of the first singlet excitation for each regioisomer at the M06-2X/def2-TZVP level of theory[35] (see the SI for full
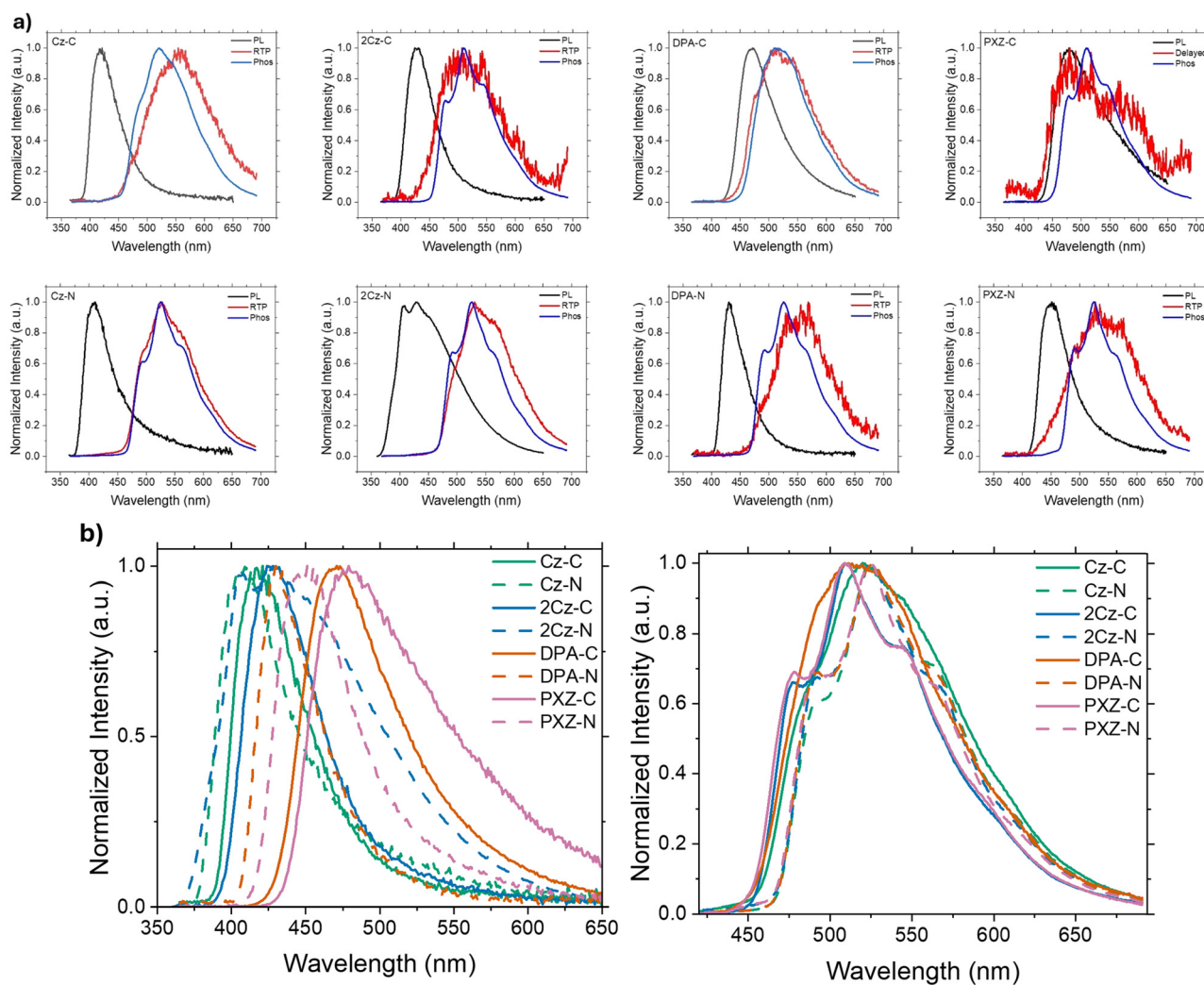

Fig. 2 (a) Steady-state photoluminescence (room temperature, under vacuum), delayed emission (room temperature, millisecond delay times, under vacuum), and phosphorescence spectra (80 K, millisecond delay times, under cold dry nitrogen stream) of the prepared emitters doped at 1 wt% in zeonex films. (b) Combined comparisons of steady-state photoluminescence (left) and 80 K phosphorescence (right).

computational details). We found the nature of this excitation differs between the N- and C-connected donors. For **DPA-C**, this excitation is predominantly a HOMO-to-LUMO transition (81%). In contrast, for **DPA-N**, the HOMO-to-LUMO contribution is only 42%, with a significant involvement of the HOMO-to-LUMO+1 transition (50%) (see Table S3, SI). Since the latter transition occurs at a higher energy, the absorption band of **DPA-N** is blue-shifted relative to **DPA-C**.

With their D–A structures initially designed to support TADF emission, the materials were investigated using time-resolved photoluminescence (PL) spectroscopy. Thin films were prepared by dispersing the compounds at 1 wt% in zeonex, capturing their intrinsic properties while minimising aggregation effects. Fig. 2 compares the steady-state PL with the time

resolved delayed emission at both room temperature and 80 K, while Fig. 3 shows the contour plots of normalised emission spectra at both room temperature and 80 K. The photoluminescence quantum yields of the materials were relatively low (2–20%) and are provided in the SI (Table S1).

Contrary to our expectations, delayed emission was only observed in a subset of the materials at room temperature, with significant variation across the series. Most emitters that exhibited delayed emission showed spectra that were strongly red-shifted from their prompt (singlet) emission and closely resembled the delayed emission measured at 80 K, which is confidently attributed to phosphorescence (PH). Based on this spectral similarity (Fig. 2a), all but one of these emitters are categorised as room temperature phosphorescence (RTP)
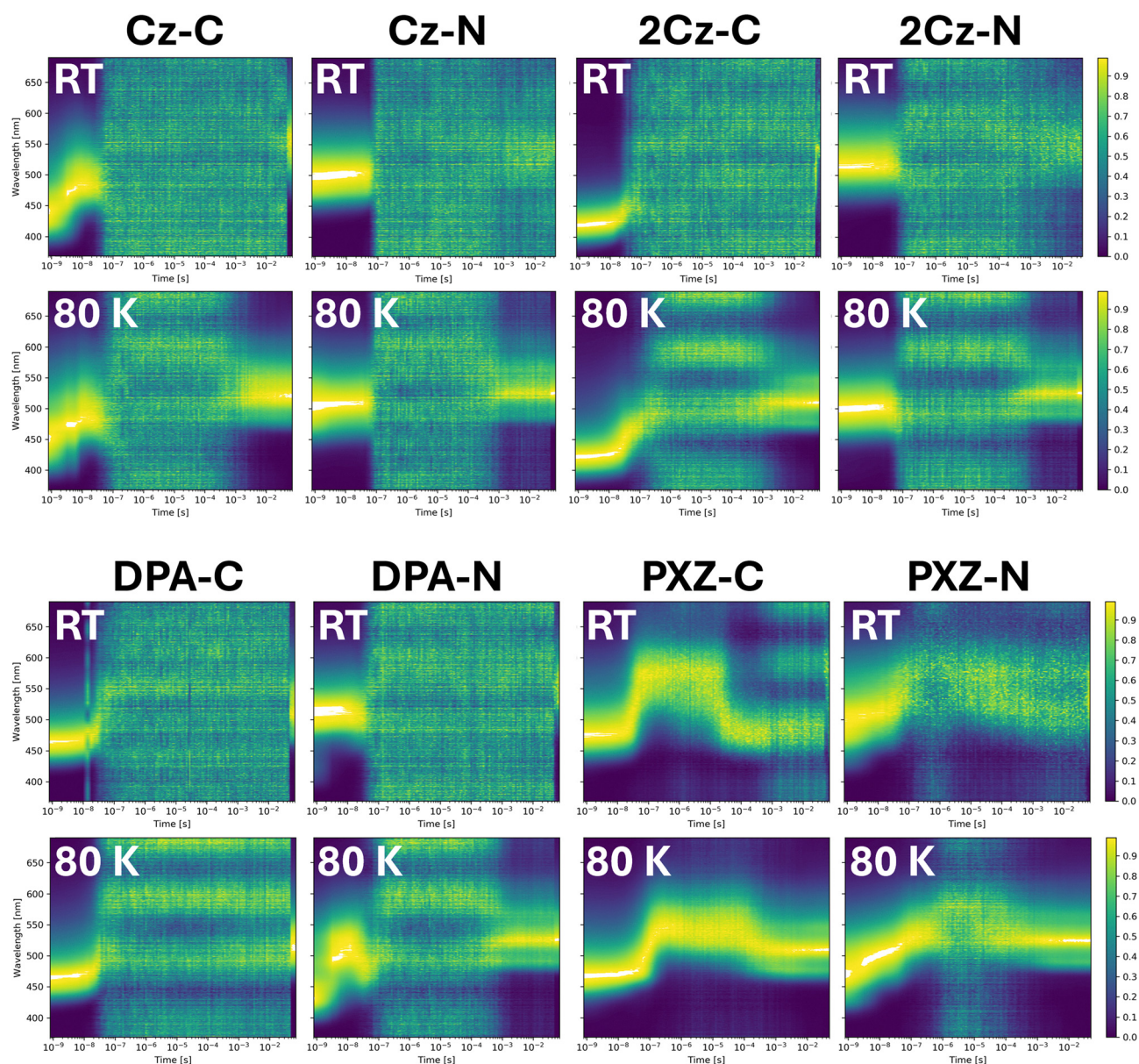

Fig. 3 Contour plots of normalised time-resolved emission spectra for the different materials (1 wt% zeonex films) at both room temperature and at 80 K. Large areas of ''flat'' spectra indicate time regions where the film emission falls below the instrument sensitivity floor.

emitters. For **PXZ-C** the delayed (millisecond-timescale) emission closely matches the prompt emission, suggesting that the long-lived emission originates from the same excited state. This behaviour is consistent with TADF, albeit with a slow decay rate and therefore low RISC rate. Notably, **PXZ-C** and **PXZ-N** exhibited an additional microsecond-timescale emission distinct from their later millisecond-timescale emission (Fig. 3), as discussed further below.

The 80 K PH spectra of the emitters (Fig. 2b, right) are closely aligned, indicating that the lowest-energy triplet state is consistently localised on the common quinoxaline acceptor. This supports our assignment of a ^{3}LE state as the origin of both the 80 K PH and 300 K RTP. To further investigate this assignment, we calculated the triplet-state electron density relative to the ground state using TDDFT (Fig. 4). In agreement with experimental findings, most emitters exhibit a T_1 state of ^{3}LE character with electron density changes predominantly localised on the quinoxaline acceptor. However, the computational results suggest that **PXZ-C** and **DPA-C** additionally show some contribution from the donor fragment, implying a potential deviation from the common ^{3}LE state. For **DPA-C**, the lowest triplet is associated with a higher ^{3}CT character, so the hybrid nature is observed (see Fig. 4) which is consistent with its unstructured (experimental) phosphorescence spectrum. The calculated T_1 electron density differences for **PXZ-C** demonstrates localisation on the donor unit, in contrast to the other materials in the series. We propose that vibrational coupling between the triplet states, enabled by their close energies (see Fig. S5 and Table S4), leads to the observed phosphorescence originating from the more emissive (^{3}LE) T_2 state, which closely resembles the T_1 states of the other emitters. Indeed, the calculated T_2 and T_3 states of **PXZ-C** show a clear localisation on the acceptor unit (Fig. S5), thus state-mixing character of this molecule is suggested.[1] Despite these observations, the 80 K phosphorescence spectra remain similar

to the rest of the series, suggesting that any donor contribution to T_1 (computational T_2) is minimal. Taken together, these results reinforce that the lowest-energy triplet state in this series is predominantly localised on the quinoxaline acceptor, with only minor variations across different donor units in the C-type connection mode.

The relatively large ΔE_{ST} values, estimated from the onset of steady-state PL at room temperature (singlet, Fig. 2b left) and the delayed emission spectra at 80 K (triplet, 80 ms, Fig. 2b right), allow us to post-hoc rationalise the predominance of RTP emission over TADF. This triplet-dominated pathway is likely assisted by the presence of N heteroatoms in the triazole linker analogous to what has been observed for thiophene-linked D–A materials.[15,16,36] The estimated and calculated values for the lowest singlet and triplet states are listed in Table S5, SI. While most compounds exhibit relatively high ΔE_{ST} values exceeding 0.4 eV, two exceptions stand out: **PXZ-C** (0.10 eV) and **DPA-C** (0.15 eV), which show significantly lower singlet energies and therefore smaller singlet–triplet energy gaps. However, only **PXZ-C** shows evidence of TADF emission (Fig. 3), while the gap in **DPA-C** appears too large to facilitate efficient RISC, instead resulting in RTP.

The onsets of the steady-state (room temperature) PL of the same donor are consistently blue-shifted for the N-connected materials (see Fig. 2b, left), indicating that their singlet energies are higher than those of their C-connected regioisomers. A similar trend is observed in TDDFT calculations for DPA- and PXZ-modified molecules, where the N-connected derivatives exhibit higher singlet energies than their C-connected counterparts (see Table S5, SI). This is consistent with the calculated LUMO orbitals (Fig. 5), where C-connected isomers show delocalisation through the entire triazole π-system, including significant density on the triazole nitrogens. This extended delocalisation lowers the LUMO energies of the C-connected series (Table 1 and SI, Table S2), resulting in reduced HOMO–LUMO gaps and red-shifted charge-transfer (CT) emission.
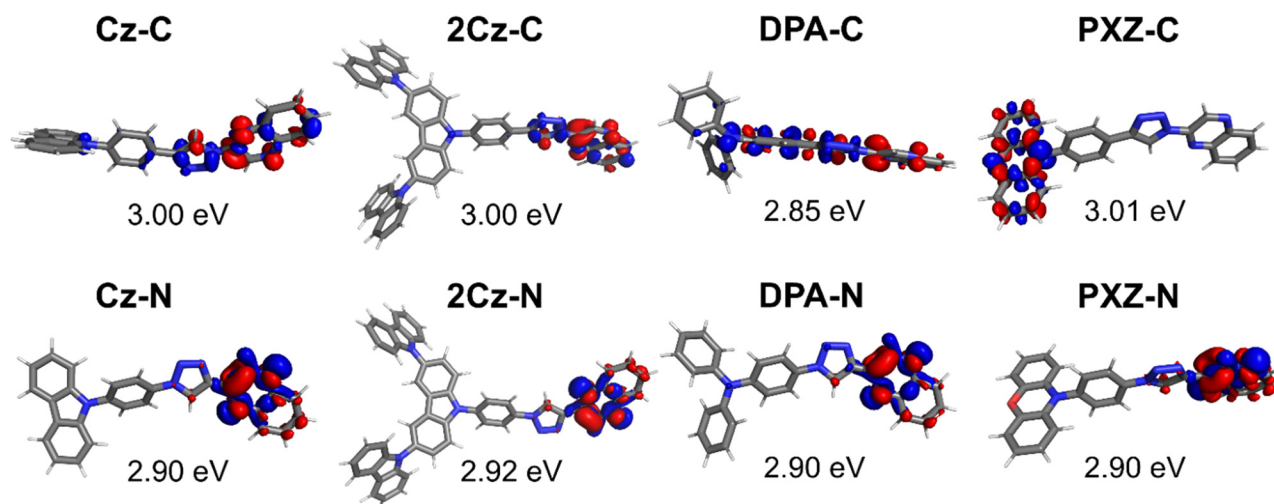

Fig. 4 Electron density difference in the lowest triplet state in comparison to the ground state. Red regions show increased electron density (accumulation), while blue regions show decreased electron density (depletion). Energy of the optimized triplets are indicated for clarity. Visualization was made with isovalue of 0.002 a.u.
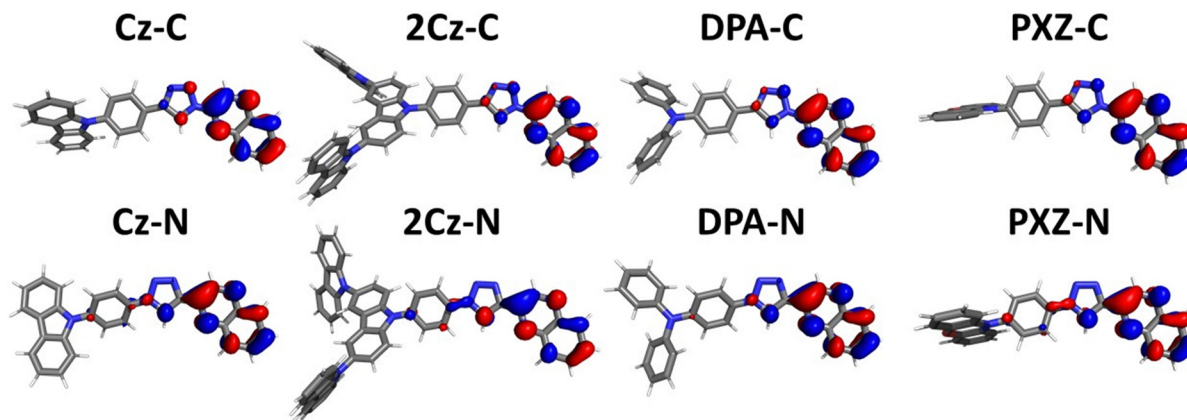
Fig. 5 Visualization of the lowest unoccupied molecular orbitals of C-connected and N-connected compounds. Visualization was made with isovalue of 0.04 a.u.

In contrast, the N-connected isomers show no LUMO density on the triazole's nitrogen linkage, confirming that conjugation is disrupted in this orientation and in agreement with the experimental PL onsets and the limited variation in LUMO energies observed by electrochemistry (Table 1). This reduced conjugation effectively weakens the electron-accepting ability of the quinoxaline unit in the N-connected series, contributing to their higher singlet energies. No significant changes were observed in the HOMO localisation (Fig. S6, SI), consistent with the HOMO levels being primarily determined by donor strength. The progressive red-shift in PL onsets across the series (Cz → 2Cz → DPA → PXZ) reflects the increasing electron-donating strength of the donor, which lowers the excited-state energies of the resulting CT states and aligns with the trends observed in the electrochemical HOMO levels.

The lower triplet energies observed for the N-connected isomers (Fig. 2b, right) can similarly be rationalised by their reduced donor–acceptor conjugation. In these materials, the nitrogen linkage disrupts π-conjugation, limiting the interaction between donor and acceptor and reducing CT character in the excited states. While this results in higher singlet CT energies due to reduced donor contribution, the lowest triplet state (^{3}LE) remains predominantly localised on the quinoxaline acceptor and is less influenced by the donor. As a result, the weaker electronic coupling in the N-connected isomers preserves the localised nature of the triplet, keeping it closer to the energy of the pure acceptor LE state. The accompanying ^{3}CT state in the N-connected systems is likely poorly coupled to the singlet, preventing efficient reverse intersystem crossing and favouring emission from the lower-lying ^{3}LE state. In contrast, the increased donor–acceptor interaction in C-connected analogues introduces some CT character into T$_1$, slightly raising its energy. This is consistent with the experimentally observed blue-shift in phosphorescence, and the trend is also reflected in the calculated triplet energies (see Table S5, SI). These observations further support the conclusions drawn from electrochemical analysis, where the small variation in LUMO energies across the N-connected series reflects weaker donor–acceptor communication, while the greater sensitivity of the

C-connected materials to donor strength is consistent with enhanced electronic coupling influencing both S$_1$ and T$_1$ state energies.

The unique microsecond-timescale delayed emission in **PXZ-C** (and to a lesser extent in **PXZ-N**) can be attributed to their aggregation properties. Among the entire series, these two emitters exhibit notably low solubility and emit in the orange-to-red region as powders (see Fig. S3, SI). This red-shifted emission as pure solids, correlated with their poor solubility, likely arises from aggregated species with lowered singlet energies. While this red emission disappears visually when the materials are dispersed in the zeonex polymer films, it is reasonable to expect that small yet spectroscopically-detectable populations of aggregates persist in these films (Fig. S4). In contrast to the excited states of the monomers, which have large ΔE_{ST} gaps (see Table S5, SI), the red-shifted singlet aggregated states likely posesses smaller ΔE_{ST} gaps to the same triplet state, potentially enabling TADF. As a result, we interpret the red-shifted delayed (microsecond timescale) emission as arising from TADF in these aggregates in thin films, though with a shorter lifetime, before it attenuates and the longer-lived monomer TADF emission becomes dominant.

Conclusion

This study demonstrates that triazole connectivity plays a critical role in governing the photophysical properties of donor–acceptor emitters. The C- and N-connected regioisomers exhibit distinct behaviours, influencing electronic coupling, charge-transfer character and delayed emission pathways. Across the series, the photophysical properties are primarily dictated by the combined effects of donor strength and triazole orientation. N-connected derivatives display higher singlet energies, consistent with decreased donor–acceptor communication and larger HOMO–LUMO gaps. In contrast, C-connected regioisomers benefit from enhanced donor–acceptor communication, facilitated by greater π-conjugation through the triazole linker. These conclusions are supported by both

3512 | *Mater. Chem. Front.*, 2025, **9**, 3505–3515

This journal is © The Royal Society of Chemistry and the Chinese Chemical Society 2025

experimental photoluminescence onsets and electrochemical LUMO levels, which vary more significantly with donor strength only in the C-connected series.

Most emitters in this study predominantly exhibit RTP, with large ΔE_{ST} values (> 0.4 eV) suppressing TADF. Notably, **PXZ-C** represents an exception, showing some delayed fluorescence at room temperature, attributed to its smaller ΔE_{ST} (0.10 eV) and enhanced CT-character. Computational and spectroscopic data confirm that the triplet state is predominantly acceptor-localised, with N-connected isomers showing slightly lower triplet energies due to reduced donor influence. Finally, the unique delayed emission behaviour observed in **PXZ-C** (and **PXZ-N**) appears to be linked to aggregation effects, consistent with their poor solubility and red-shifted solid-state emission.

Overall, these findings underscore the importance of regioisomeric control in the design of D–A emissive materials, offering valuable insight into how triazole connectivity can be leveraged to tune excited-state properties and emission pathways. In future designs, combining strong donors with C-connected triazoles, alongside systematic tuning of the acceptor unit, may provide a viable strategy to further reduce ΔE_{ST} and expand the scope of efficient TADF emitters.

Conflicts of interest

There are no conflicts to declare.

Data availability

Supplementary information (SI): the SI covers detailed descriptions of the conducted experiments, as well as the quantum mechanical calculations and their results. It includes all experimental and computational details, including the analytical data for the obtained target compounds and byproducts. See DOI: https://doi.org/10.1039/d5qm00572h.

Data that refers to the experiments described herein were submitted to the repository Chemotion (https://www.chemotion-repository.net/). All DOIs minted for the data are linked in the SI. New data obtained in this study is assigned to the collection embargo number LSH_2024-07-09 (https://dx.doi.org/10.14272/collection/LSH_2024-07-09). The material obtained in this study was submitted to the Molecule Archive at KIT and can be requested from there (https://compound-platform.eu/home). The files generated during quantum chemical calculations are available at https://dx.doi.org/10.17172/NOMAD/2025.07.18-1.

CCDC 2374289 (**DPA-N**), 2374290 (**PXZ-N**), 2374291 (**DPA-C**) and 2374292 (**PXZ-C**) contain the supplementary crystallographic data for this paper.[37a–d]

Acknowledgements

References

1 J. M. dos Santos, D. Hall, B. Basumatary, M. Bryden, D. Chen, P. Choudhary, T. Comerford, E. Crovini, A. Danos, J. De, S. Diesing, M. Fatahi, M. Griffin, A. K. Gupta, H. Hafeez, L. Hämmerling, E. Hanover, J. Haug, T. Heil, D. Karthik, S. Kumar, O. Lee, H. Li, F. Lucas, C. F. R. Mackenzie, A. Mariko, T. Matulaitis, F. Millward, Y. Olivier, Q. Qi, I. D. W. Samuel, N. Sharma, C. Si, L. Spierling, P. Sudhakar, D. Sun, E. Tankelevičiutė, M. D. Tonet, J. Wang, T. Wang, S. Wu, Y. Xu, L. Zhang and E. Zysman-Colman, The Golden Age of Thermally Activated Delayed Fluorescence Materials: Design and Exploitation, *Chem. Rev.*, 2024, **124**, 13736–14110.

2 D. Chen, J. Gong, J. Grüne, T. Matulaitis, A. J. Gillett, X. H. Zhang, I. D. W. Samuel, G. A. Turnbull and E. Zysman-Colman, Tetra-Donor Pyrazine Based Thermally Activated Delayed Fluorescence Emitters for Electroluminescence and Amplified Spontaneous Emission, *Adv. Func. Mater.*, 2024, **34**, 2409592.

3 X. Zhen, Y. Tao, Z. An, P. Chen, C. Xu, R. Chen, W. Huang and K. Pu, Ultralong Phosphorescence of Water-Soluble Organic Nanoparticles for In Vivo Afterglow Imaging, *Adv. Mater.*, 2017, **29**, 1606665.

4 A. J. Gillett, A. Pershin, R. Pandya, S. Feldmann, A. J. Sneyd, A. M. Alvertis, E. W. Evans, T. H. Thomas, L. S. Cui, B. H. Drummond, G. D. Scholes, Y. Olivier, A. Rao, R. H. Friend and D. Beljonne, Dielectric control of reverse intersystem crossing in thermally activated delayed fluorescence emitters, *Nat. Mater.*, 2022, **21**, 1150–1157.

5 N. Mallo, S. McAnally, H. Jin, E. Brooks, R. Chu, M. Babazadeh, J. Smyth, D. M. Huang, N. Hight-Huf, O. G. Reid, G. Rumbles and P. L. Burn, I. R. Gentle and P. E. Shaw, Free-Charge Carrier Generation in Homojunction Non-Polymeric Organic Semiconductor Films – The Role of the Optical Frequency Dielectric Constant, *Adv. Opt. Mater.*, 2024, **12**, 2401825.

6 W. Jiang, H. Jin, M. Babazadeh, A. S. Loch, A. Raynor, N. Mallo, D. M. Huang, X. Jiao, W. L. Tan, C. R. McNeill, P. L. Burn and P. E. Shaw, Dielectric Constant Engineering of Organic Semiconductors: Effect of Planarity and Conjugation Length, *Adv. Funct. Mater.*, 2021, **32**, 2104259.

7 J. S. Ward, A. Danos, P. Stachelek, M. A. Fox, A. S. Batsanov, A. P. Monkman and M. R. Bryce, Exploiting trifluoromethyl substituents for tuning orbital character of singlet and triplet states to increase the rate of thermally activated delayed fluorescence, *Mater. Chem. Front.*, 2020, **4**, 3602–3615.

8 N. A. Kukhta, H. F. Higginbotham, T. Matulaitis, A. Danos, A. N. Bismillah, N. Haase, M. K. Etherington, D. S. Yufit, P. R. McGonigal, J. V. Gražulevičius and A. P. Monkman, Revealing resonance effects and intramolecular dipole interactions in the positional isomers of benzonitrile-core thermally activated delayed fluorescence materials, *J. Mater. Chem. C*, 2019, **7**, 9184–9194.

9 F.-M. Xie, J.-X. Zhou, Y.-Q. Li and J.-X. Tang, Effects of the relative position and number of donors and acceptors on the properties of TADF materials, *J. Mater. Chem. C*, 2020, **8**, 9476–9494.

10 P. Govindharaj, A. J. Wierzba, K. Keska, M. A. Kochman, G. Wiosna-Salyga, A. Kubas, P. Data and M. Lindner, Regioisomerism vs Conformation: Impact of Molecular Design on the Emission Pathway in Organic Light-Emitting Device Emitters, *ACS Appl. Mater. Interfaces*, 2024, **16**, 23654–23667.

11 G. Haykir, M. Aydemir, A. Danos, S. Gumus, G. Hizal, A. P. Monkman and F. Turksoy, Effects of asymmetric acceptor and donor positioning in deep blue pyridyl-sulfonyl based TADF emitters, *Dyes Pigm.*, 2021, **194**, 109579.

12 G. Haykir, M. Aydemir, A. Tekin, E. Tekin, A. Danos, F. Yuksel, G. Hizal, A. P. Monkman and F. Turksoy, Effects of donor position and multiple charge transfer pathways in asymmetric pyridyl-sulfonyl TADF emitters, *Mater. Today Commun.*, 2022, **31**, 103550.

13 S. K. Pathak, G. Li, C. Zhou, Z. Wang and H. Liu, Regio-isomer enabling efficient red TADF emitters based on pyridobenzoquinoxaline, *J. Mater. Chem. C*, 2023, **11**, 6685–6694.

14 S. Brebels, T. Cardeynaels, L. Jackers, S. Kuila, H. Penxten, R. J. Salthouse, A. Danos, A. P. Monkman, B. Champagne and W. Maes, Isomeric modulation of thermally activated delayed fluorescence in dibenzo[a,c]phenazine-based (deep) red emitters, *J. Mater. Chem. C*, 2024, **12**, 9255–9265.

15 S. Paredis, T. Cardeynaels, J. Deckers, A. Danos, D. Vanderzande, A. P. Monkman, B. Champagne and W. Maes, Bridge control of photophysical properties in benzothiazole-phenoxazine emitters – from thermally activated delayed fluorescence to room temperature phosphorescence, *J. Mater. Chem. C*, 2022, **10**, 4775–4784.

16 S. Paredis, T. Cardeynaels, S. Kuila, J. Deckers, M. Van Landeghem, K. Vandewal, A. Danos, A. P. Monkman, B. Champagne and W. Maes, Balanced Energy Gaps as a Key Design Rule for Solution-Phase Organic Room Temperature Phosphorescence, *Chem. – Eur. J.*, 2023, **29**, e202301369.

17 A. Danos, D. Gudeika, N. A. Kukhta, R. Lygaitis, M. Colella, H. F. Higginbotham, A. N. Bismillah, P. R. McGonigal, J. V. Grazulevicius and A. P. Monkman, Not the sum of their parts: understanding multi-donor interactions in symmetric and asymmetric TADF emitters, *J. Mater. Chem. C*, 2022, **10**, 4737–4747.

18 S. Kothavale, S. C. Kim, K. Cheong, S. Zeng, Y. Wang and J. Y. Lee, Solution-Processed Pure Red TADF Organic Light-Emitting Diodes With High External Quantum Efficiency and Saturated Red Emission Color, *Adv. Mater.*, 2023, **35**, 2208602.

19 J. Liang, C. Li, Y. Cui, Z. Li, J. Wang and Y. Wang, Rational design of efficient orange-red to red thermally activated delayed fluorescence emitters for OLEDs with external quantum efficiency of up to 26.0% and reduced efficiency roll-off, *J. Mater. Chem. C*, 2020, **8**, 1614–1622.

20 X. Li, Y. Chen, S. Li, A. Li, L. Tu, D. Zhang, L. Duan, Y. Xie, B. Z. Tang and Z. Li, Quinoxaline-based thermally activated delayed fluorescence emitters for highly efficient organic light-emitting diodes, *J. Mater. Chem. C*, 2023, **11**, 5217–5224.

21 Z. Li, D. Yang, C. Han, B. Zhao, H. Wang, Y. Man, P. Ma, P. Chang, D. Ma and H. Xu, Optimizing Charge Transfer and Out-Coupling of A Quasi-Planar Deep-Red TADF Emitter: towards Rec.2020 Gamut and External Quantum Efficiency beyond 30, *Angew. Chem., Int. Ed.*, 2021, **60**, 14846–14851.

22 L. Yu, Z. Wu, G. Xie, W. Zeng, D. Ma and C. Yang, Molecular design to regulate the photophysical properties of multi-functional TADF emitters towards high-performance TADF-based OLEDs with EQEs up to 22.4% and small efficiency roll-offs, *Chem. Sci.*, 2018, **9**, 1385–1391.

23 F. M. Xie, J. X. Zhou, X. Y. Zeng, Z. D. An, Y. Q. Li, D. X. Han, P. F. Duan, Z. G. Wu, Y. X. Zheng and J. X. Tang, Efficient Circularly Polarized Electroluminescence from Chiral Thermally Activated Delayed Fluorescence Emitters Featuring Symmetrical and Rigid Coplanar Acceptors, *Adv. Opt. Mater.*, 2021, **9**, 2100017.

24 Y. Chen, D. Zhang, Y. Zhang, X. Zeng, T. Huang, Z. Liu, G. Li and L. Duan, Approaching Nearly 40% External Quantum Efficiency in Organic Light Emitting Diodes Utilizing a Green Thermally Activated Delayed Fluorescence Emitter with an Extended Linear Donor-Acceptor-Donor Structure, *Adv. Mater.*, 2021, **33**, 2103293.

25 X. Gong, P. Li, Y. H. Huang, C. Y. Wang, C. H. Lu, W. K. Lee, C. Zhong, Z. Chen, W. Ning, C. C. Wu, S. Gong and C. Yang, A Red Thermally Activated Delayed Fluorescence Emitter Simultaneously Having High Photoluminescence Quantum Efficiency and Preferentially Horizontal Emitting Dipole Orientation, *Adv. Funct. Mater.*, 2020, **30**, 1908839.

26 E. V. Puttock, C. S. K. Ranasinghe, M. Babazadeh, J. Jang, D. M. Huang, Y. Tsuchiya, C. Adachi, P. L. Burn and P. E. Shaw, Solution-Processed Dendrimer-Based TADF Materials for Deep-Red OLEDs, *Macromolecules*, 2020, **53**, 10375–10385.

27 A. S. Cornec, C. Baudequin, C. Fiol-Petit, N. Plé, G. Dupas and Y. Ramondenc, One ''Click'' to Access Push–Triazole–Pull Fluorophores Incorporating a Pyrimidine Moiety: Structure–Photophysical Properties Relationships, *Eur. J. Org. Chem.*, 2013, 1908–1915.

28 P. Kautny, D. Bader, B. Stoger, G. A. Reider, J. Frohlich and D. Lumpi, Structure-Property Relationships in Click-Derived Donor-Triazole-Acceptor Materials, *Chem. – Eur. J.*, 2016, **22**, 18887–18898.

29 F. K. Merkt, K. Pieper, M. Klopotowski, C. Janiak and T. J. J. Muller, Sequential Cu-Catalyzed Four- and Five-Component Syntheses of Luminescent 3-Triazolylquinoxalines, *Chem. – Eur. J.*, 2019, **25**, 9447–9455.

30 A. Wild, C. Friebe, A. Winter, M. D. Hager, U. W. Grummt and U. S. Schubert, π-Conjugated 2,2′:6′,2″-Bis(terpyridines): Systematical Tuning of the Optical Properties by Variation of the Linkage between the Terpyridines and the π-Conjugated System, *Eur. J. Org. Chem.*, 2010, 1859–1868.

31 C. Müller, S. Bold, M. Chavarot-Kerlidou and B. Dietzek-Ivanšić, Photoinduced electron transfer in triazole-bridged donor-acceptor dyads – A critical perspective, *Coord. Chem. Rev.*, 2022, **472**, 214764.

32 C. M. Cardona, W. Li, A. E. Kaifer, D. Stockdale and G. C. Bazan, Electrochemical considerations for determining absolute frontier orbital energy levels of conjugated polymers for solar cell applications, *Adv. Mater.*, 2011, **23**, 2367–2371.

33 T. Yanai, D. P. Tew and N. C. Handy, A new hybrid exchange–correlation functional using the Coulomb-attenuating method (CAM-B3LYP), *Chem. Phys. Lett.*, 2004, **393**, 51–57.

34 F. Weigend and R. Ahlrichs, Balanced basis sets of split valence, triple zeta valence and quadruple zeta valence quality for H to Rn: Design and assessment of accuracy, *Phys. Chem. Chem. Phys.*, 2005, **7**, 3297–3305.

35 Y. Zhao and D. G. Truhlar, The M06 suite of density functionals for main group thermochemistry, thermochemical kinetics, noncovalent interactions, excited states, and transition elements: two new functionals and systematic testing of four M06-class functionals and 12 other functionals, *Theor. Chem. Acc.*, 2008, **120**, 215–241.

36 H. Marchi Luciano, G. Farias, C. M. Salla, L. G. Franca, S. Kuila, A. P. Monkman, F. Durola, I. H. Bechtold, H. Bock and H. Gallardo, Room Temperature Phosphorescence in Solution from Thiophene-Bridged Triply Donor-Substituted Tristriazolotriazines, *Chem. – Eur. J.*, 2023, **29**, e202203800.

37 (*a*) CCDC 2374289: Experimental Crystal Structure Determination, 2025, DOI: **10.5517/ccdc.csd.cc2kpmzw**; (*b*) CCDC 2374290: Experimental Crystal Structure Determination, 2025, DOI: **10.5517/ccdc.csd.cc2kpn0y**; (*c*) CCDC 2374291: Experimental Crystal Structure Determination, 2025, DOI: **10.5517/ccdc.csd.cc2kpn1z**; (*d*) CCDC 2374292: Experimental Crystal Structure Determination, 2025, DOI: **10.5517/ccdc.csd.cc2kpn20**.